Temperature dependence of the local structure of $YBa_2Cu_3O_{7-\delta}$ with varying oxygen content: An x-ray-absorption study

J. B. Boyce
Xerox Palo Alto Research Center, Palo Alto, California 94304

F. Bridges
Department of Physics, University of California, Santa Cruz, California 95064

T. Claeson
Physics Department, Chalmers University of Technology, S-41296 Gothenburg, Sweden

M. Nygren
Arrhenius Laboratory, Stockholm University, S-10691 Stockholm, Sweden
(Received 21 October 1988)

The local structure of $YBa_2Cu_3O_y$ determined using x-ray-absorption fine structure (XAFS) agrees well with the long-range order given by diffraction results for both oxygen-rich, orthorhombic ($y=6.98$ and 6.87) and oxygen-deficient, tetragonal ($y=6.15$) compounds. The x-ray-absorption near-edge structure supports the conclusion that, as $y=7$ goes to $y=6$, the O is removed from the chains and the chain Cu atoms, Cu(1), becomes monovalent with a linear O-Cu-O structural configuration and a $3d^{10}$ electronic configuration, as in Cu_2O. For the XAFS analysis, structural standards were determined, and these standards worked well not only for the Cu first-neighbor O environment but also for the Cu second-neighbor metal-atom environment out to 4 Å. A detailed multipeak analysis reproduced the XAFS spectra well and yielded structural parameters that agree with diffraction. The temperature dependence of the structural parameters shows only a smooth variation, with no significant anomalies. The Cu-X distances have a negligible to a small positive change with temperature, consistent with the lattice expansion. The exception is the Cu-Ba distances which change substantially; the Cu(1)-Ba distance increases and the Cu(2)-Ba distance decreases. This indicates that the Ba moves away from the Cu(1)-O chains and toward the Cu(2)-O planes with increasing temperature and that anharmonicity plays a role. This motion is larger for the oxygen-depleted compound than for the fully oxygenated material. The in-plane Cu-O first-neighbor vibrations exhibit no significant softening with temperature. They agree well with a harmonic, Einstein oscillator model which shows that the Cu−O bonds are tightly bound (characteristic Einstein temperatures $\Theta_E=596\pm20$ K) and are slightly softer by 6% in the oxygen-deficient, tetragonal material.

I. INTRODUCTION

Small perturbations of the structure and composition of the 90-K superconductor $YBa_2Cu_3O_y$ (Y-Ba-Cu-O) can have profound effects on its superconducting properties.[1] To elucidate the relationship between the local structure of Y-Ba-Cu-O and its superconducting properties, we have studied oxygen-rich ($y=7-\delta\approx7$) and oxygen-deficient ($y=7-\delta\approx6$) Y-Ba-Cu-O compounds by x-ray-absorption spectroscopy.

The structure of $YBa_2Cu_3O_{7-\delta}$ is a distorted, oxygen-deficient, trilayer perovskite,[2-12] which as a 90-K superconductor ($\delta<0.2$) is orthorhombic with two distinct Cu sites: two Cu(2) sites and one Cu(1) site, corresponding to two-dimensional Cu-O planes and one-dimensional Cu-O chains, respectively. Since our discussion centers around the location of the atoms in this material, we show this much-discussed structure in Fig. 1. The notation for the atoms is that given in Ref. 10 for both the orthorhombic and tetragonal phases. The Cu(2)-O layers in the a-b plane form a mainly square, but slightly puckered, two-dimensional Cu lattice with oxygen atoms situated midway between each nearest neighbor pair. These layers are separated by Y layers that contain no oxygen. The Cu(1)-O atoms form chains running in the b direction between two Ba-O planes. When oxygen is removed from the sample, it is the O(1) site in the Cu(1)-O chains that is depleted. As the oxygen content of the sample decreases, the oxygen defects that drive the formation of the Cu-O chains become disordered and T_c decreases. For δ greater than about 0.5 (depending on the thermal treatment), the layer is further depleted of oxygen, an orthorhombic-to-tetragonal transition takes place, and superconductivity is lost. Whether the orthorhombic distortion, consistent with the presence of one-dimensional Cu-O chains, is fundamental to the mechanism of 90-K superconductivity remains under debate.

The x-ray absorption fine structure (XAFS) is well-suited for a direct determination of the local environment of absorbing atoms.[13-15] The near-edge structure may be used to study the valence of the absorber and the electronic configuration. Furthermore, the temperature depen-

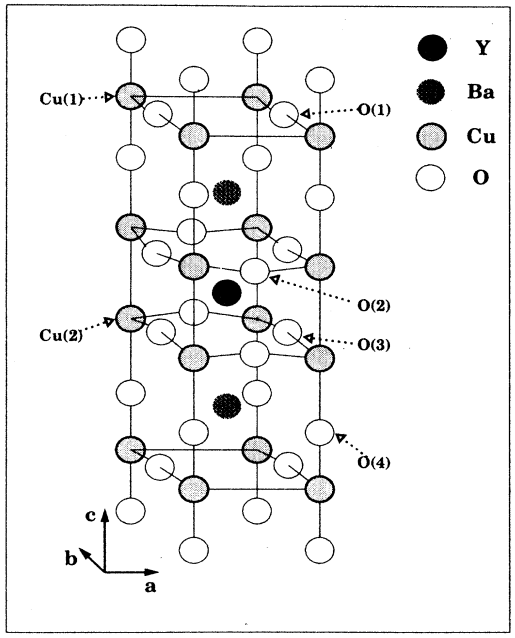

FIG. 1. The structure of $YBa_2Cu_3O_{7-\delta}$ for $\delta=0$, the fully oxygenated case ($y=7$). The notation for the atomic sites is from Jorgensen *et al.* (Ref. 10). For $\delta=1$ ($y=6$), the O(1) are fully depleted and the *a* and *b* axes are equivalent.

dence of the XAFS can yield information on any structural phase transitions that occur and on the local vibrations in the solid. To data a number of x-ray-absorption studies have been performed on the high-temperature superconductors,[16–37] and, in particular, on Y-Ba-Cu-O.[20–37] They have addressed various issues and have often arrived at conflicting conclusions. One area where there is no consensus is that of the Cu valence,[17–30,36] which we do not emphasize here. Another is that of the local structure and atomic vibrations in Y-Ba-Cu-O, which is the main topic of this work. Some XAFS studies have arrived at local metal-O environments that agree with diffraction results[21,28,31,32] and others that disagree.[23,30] For example, one XAFS study[23] has concluded that O atoms do reside in the Y plane, contrary to the diffraction results. Another[30] concluded that 20%–30% of the Cu atoms are on Y sites. In addition, some analyses of XAFS data have concluded that anomalies occur in the temperature dependence of the atomic vibrations in the vicinity of T_c and even higher.[26,31] Other studies observe no anomalies.[21,28,34]

In this paper we have performed a detailed analysis of the local environment around the Cu atoms in well-characterized Y-Ba-Cu-O out to 4 Å. This includes not only the O first neighbors but also the metal-atom second neighbors. The data have been thoroughly analyzed to obtain the local structure. These measurements have been performed as a function of temperature from 4 to 600 K with a dense set of temperature points in order to observe any sharp anomalies that may exist. In addition, results have been obtained for both fully-oxygenated ($y\approx 7$) and oxygen-deficient ($y\approx 6$) Y-Ba-Cu-O samples to contrast the two cases. Results on the Y-O near neighbor environment are also reported. Our intent is to account for the features in the data in a rigorous way and thereby try to resolve some of the controversies surrounding the interpretation of the XAFS results. To this end we emphasize two areas: (1) the detailed analysis of the local structure out to 4 Å from the Cu atoms to be able to explain all the features in the data, including the significant differences in the XAFS data for low-O and high-O samples; (2) the results on the XAFS for both low-O and high-O samples measured over a large temperature range with sufficient data in the temperature regions where anomalies have been reported to help resolve the conflicting reports.

In Sec. II we present the experimental details and in Sec. III the near-edge results. In Sec. IV the XAFS analysis of the first-neighbor oxygen atoms and second-neighbor metal atoms is presented, along with the results as a function of temperature. Section V presents a summary.

II. EXPERIMENTAL DETAILS

A. Samples

Three $YBa_2Cu_3O_y$ samples with different oxygen content were studied: $y=6.98$, 6.87, and 6.15. The $y=6.87$ compound was prepared in the "normal" way by annealing at 800 °C in one atmosphere of oxygen, followed by a slow cooling. The fully oxygenated sample, $y=6.98$, was obtained by an anneal in high oxygen pressure, 100 atmospheres. The low-oxygen content sample resulted from an anneal in N_2 at 900 °C, followed by a fast cooling. The oxygen content was determined thermogravimetrically. Diffraction measurements indicated that the samples are single phase within a few percent. The two high-O samples are orthorhombic, whereas the low-O sample is tetragonal. Note that a slightly orthorhombic compound, twinned on a scale of ≈ 10 Å, could not have been distinguished from a tetragonal compound in the x-ray diffraction. Both orthorhombic samples have a superconducting transition temperature of approximately 90 K, whereas the tetragonal material is not superconducting down to 4.2 K. In addition, powders of the following structural and x-ray near-edge standards were also prepared and characterized: Cu_2O, CuO, $KCuO_2$, a Ba-Cu oxide, and $KNa_4[Cu(HIO_6)_2]\cdot 12H_2O$.

The samples were ground into fine powders and brushed onto tapes which were stacked together to give approximately two x-ray absorption lengths at the Cu *K* edge. Each sample was selected to be free of pinholes; an x-ray photograph of each sample was taken at the synchrotron to check this selection process.

B. X-ray absorption measurements

The x-ray absorption data were collected at the Cu *K* edge (8980 eV) and Y *K* edge (17080 eV) on the wiggler beamline VII-3 at the Stanford Synchrotron Radiation Laboratory during dedicated operation (3 GeV beam energy, 30–100 mA beam current). A Si(400) double monochromator with an exit slit height of 1 mm was used.

This monochromator and optical arrangement gave an energy resolution at the Cu K edge of about 1 eV, substantially better than that of 1.9 eV for Si(220) and 3.6 eV for Si(111). The double monochromator was detuned on its rocking curve to approximately one half of maximum transmitted x-ray intensity to reduce the harmonic content of the beam to negligible levels for these experiments. A leveling feedback system was used to control the piezoelectric crystal of the monochromator to keep the incident photon flux constant.[38] For the very narrow rocking curve of the Si(400) crystals, this feedback scheme is crucial to remain on the rocking curve over a 1.5-keV scan in energy for the fine-structure measurements. All absorption measurements were taken in the transmission mode at the Cu K edge for temperatures from 4 to 600 K and at the Y K edge at 83, 170, and 300 K. The incident and transmitted x-ray intensities were measured using gas ionization counters containing N_2 gas. Simultaneously, a third such counter measured the intensity transmitted through a Cu (or Y) metal foil which was used to insure that the monochromator remained in calibration from one scan to another. The metal-foil data were used to set the energy scale for all the scans of the Y-Ba-Cu-O samples and standards. The samples were mounted in an Oxford variable flow helium dewar for the measurements from 4 to 300 K and in a furnace for the measurements from 300 to 600 K. The temperature was measured and controlled to better than 2 K for all the scans.

C. XAFS data analysis

The reduction and analysis of the XAFS data were performed in the usual way.[14,21,39–41]. First, a polynomial or spline fit to the pre-edge data is subtracted from the entire data set. Then a spline fit to the data above the absorption edge is used to remove the background from the XAFS oscillations, and the energy data converted to k-space data, $k\chi(k)$, using $k=[2m(E-E_0)]^{1/2}/\hbar$, where $\chi(k)$ is defined by the equation $\mu(k)=\mu_0[1+\chi(k)]$, μ_0 is the absorption at the step, E_0 is the edge position and $\mu(k)$ is the k-dependent absorption coefficient. Finally, a fast Fourier transform is applied to obtain the complex, r-space data, $\{F[k^n\chi(k)]\}$. Values of $n=1$ and $n=3$ were used in the analysis presented here, with $n=1$ being the most-used value.

For a quantitative comparison, data in real space were fit to structural standards in order to determine the number of neighbors at specific distances and spreads in distance with temperature. For the Y environment, only the first-neighbor oxygen atoms were analyzed. The analysis of this Y K-edge data is as described in Ref. 21. The Cu K-edge data were more thoroughly studied here, being analyzed out to 4 Å, and so we discuss this analysis in more detail. First, we describe the Cu local structure and discuss the procedure for dealing with the two inequivalent Cu sites.

In Y-Ba-Cu-O, the Cu atoms have O, Y, Ba, and Cu neighbors at the distances given in Table I. We divide the region out to 4 Å into two parts: (1) the first-neighbor region consisting of O atoms at distances of <2.5 Å and (2) a second-neighbor region between 3- and 4-Å spacing, dominated by the metal atoms. For the purposes of XAFS discussion we combine into a single peak those peaks of the same kind of neighbor that are too close for the XAFS to resolve in this complex structure, i.e., those within about 0.05 Å of each other. This reduces the num-

TABLE I. The room-temperature near-neighbor distances and number of neighbors around the Cu(1) and Cu(2) atoms in orthorhombic $YBa_2Cu_3O_7$ and tetragonal $YBa_2Cu_3O_6$ within a radius of 4 Å. For tetragonal $YBa_2Cu_3O_6$, O(1) of the orthorhombic structure is missing and O(2) and O(3) are equivalent. The notation is from Jorgensen *et al.* (Ref. 10) (Fig. 1), the structure for $y=7$ from Beno *et al.* (Ref. 3), and the structure for $y=6$ from Torardi *et al.* (Ref. 9). The average numbers are the weighted averages used in comparisons with the XAFS results.

	High O ($y=7$)				Low O ($y=6$)			
Cu-X pair	No.	r (Å)	Average no.	Average r (Å)	No.	r (Å)	Average no.	Average r (Å)
Cu(1)-O(4)	2	1.85	2/3	1.85	2	1.79	2/3	1.79
Cu(1)-O(1)	2	1.94			0	. . .		
Cu(2)-O(2)	2	1.93	10/3	1.94	4	1.94	8/3	1.94
Cu(2)-O(3)	2	1.96			. . .	. . .		
Cu(2)-O(4)	1	2.30	2/3	2.30	1	2.46	2/3	2.46
Cu(2)-O(2)	2	3.66	8/3	3.66	4	3.62	8/3	3.62
Cu(2)-O(3)	2	3.65			. . .	. . .		
Cu(2)-Y	4	3.20	8/3	3.20	4	3.18	8/3	3.18
Cu(2)-Ba	4	3.38	8/3	3.38	4	3.35	8/3	3.35
Cu(1)-Ba	8	3.47	8/3	3.47	8	3.57	8/3	3.57
Cu(2)-Cu(2)	1	3.37	2/3	3.37	1	3.29	2/3	3.29
Cu(2)-Cu(2)	2	3.82			4	3.85		
Cu(2)-Cu(2)	2	3.88	4	3.85	. . .	. . .	4	3.85
Cu(1)-Cu(1)	2	3.82			4	3.85		
Cu(1)-Cu(1)	2	3.88			. . .	. . .		

ber of peaks for $r < 4$ Å from 15 to 9 for the orthorhombic materials and from 10 to 9 for the low-O tetragonal samples. So, for example, the Cu-O in-plane distances of 1.93, 1.94, and 1.96 Å cannot be resolved and become a single peak at the weighted-average distance of 1.94 Å. Weighted averages[40] must be used since XAFS, being a bulk probe, sees a superposition of all pairs in an unoriented powdered sample. This weighing must include not only the number of neighboring atoms but also the number of Cu central atoms since there are two inequivalent Cu sites: one Cu(1) and two Cu(2). Since the Cu XAFS is normalized to the number of Cu central atoms, the number of neighbors must be normalized in a similar fashion. So, for example, the weighted number of O neighbors at 1.85 Å in the high-O sample is two Cu(1)-O(4) pairs times the fraction of the Cu atoms that contribute to this distance, $\frac{1}{3}$. The weighted-average number of O atoms at this distance is then $\frac{2}{3}$, as shown in Table I along with the weighted-average number of X atoms for the other Cu-X pairs. These are the pertinent number of neighbors for the XAFS analysis.[40]

The structural standards for each of the four different Cu-X pairs were determined in the following manner. For the Cu-O peaks, Cu_2O was used. Cu_2O has two O neighbors to each Cu at 1.85 Å and twelve Cu second neighbors at 3.02 Å. To ensure that the small Cu-O peak in the standard was not effected by overlap from the larger Cu-Cu peak, a Cu-Cu peak using a Cu-metal standard was fit to the second neighbor in Cu_2O and the result subtracted from the Cu_2O data. The resulting spectrum differed only slightly from the raw data in the region of the O peak, indicating that interference between the O and Cu first and second neighbors is small in the standard. This Cu-O standard was then applied in a three-Gaussian fit to the first-neighbor region of the Y-Ba-Cu-O data. The three parameters for each Gaussian are the weighted-average number of neighbors (N), the pair separation (r), and the peak width or Debye-Waller factor (σ). They were all varied with the constraint that the ratio of the N's be the same as that from diffraction. This constraint reduced the number of parameters by two. Fits allowing the threshold energy E_0 to vary were also performed and yielded similar results since the resulting shifts for a best fit were small, $|\Delta E_0| \leq 2$ eV. Also fits both without and with a mean free path of $\lambda \approx 8$ Å gave similar results since the differences in distances between the standards and unknowns are $\ll\lambda$. Good fits were obtained, reproducing the diffraction structural parameters (Table I), as discussed below.

For the second-neighbor Cu-metal atom pairs, an experimental standard was available for Cu-Cu, namely Cu metal, but not for Cu-Y and Cu-Ba. For these two pairs, the following procedure was used to obtain a standard for the amplitudes and phases. First, experimental data of pairs of atoms close to the unknown pair of interest were obtained. For example, zinc-blende-structured CuI where the Cu central atoms have four iodine neighbors at 2.61 Å was used to obtain the standard for Cu-Ba. For this structure, the Cu-I peak is well isolated and Fourier filtering has a minimal effect on the real-space spectrum since the low-r tails of more distant neighbors makes a negligible contribution. The Cu-I ($Z=53$) data were modified using spherical wave calculations[42] to correct for the small difference in Z to Cu-Ba ($Z=56$). This procedure then relies mainly on experimental standards, using the theoretical calculations only to interpolate the amplitudes and phases a small distance in Z from 53 to 56. Since, for spherical waves, the amplitudes and phases depend on distance, the difference in near-neighbor spacing from 2.61 Å for Cu-I to about 3.4 Å for Cu-Ba was also taken into account. Figure 2 shows the Fourier-filtered first-neighbor peak in CuI and the resulting spectrum for Cu-Ba. Both the k-space and r-space spectra are shown. The Cu-Ba spectrum is for four Ba neighbors at 2.61 Å as for CuI so that amplitude and phase differences in this figure are due only to the difference in backscatterer, i.e., $Z=53$ vs $Z=56$. For the comparisons with the Y-Ba-Cu-O data,

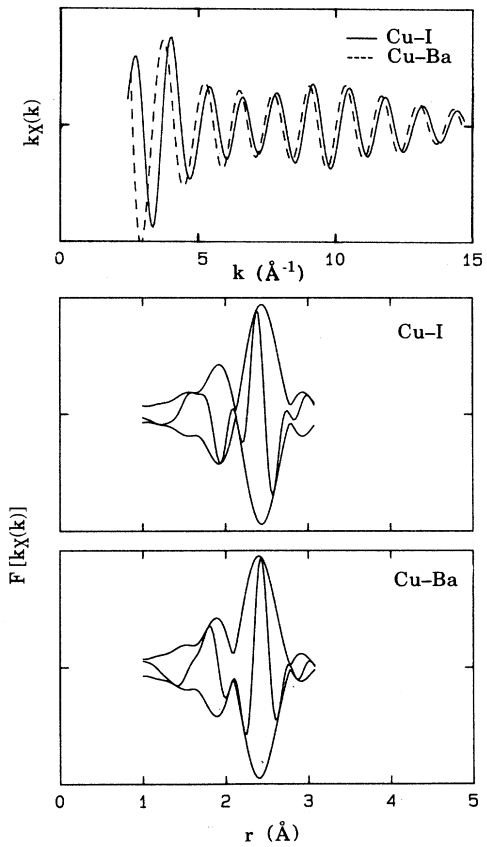

FIG. 2. Fourier-filtered first-neighbor peak in CuI and the spectrum for Cu-Ba obtained from CuI, as described in the text. The upper curve is the k-space spectra and the lower two curves are the r-space spectra, where the envelope curve is the magnitude of the complex transform (plotted as $+|F[k\chi(k)]|$ and $-|F[k\chi(k)]|$) and the oscillatory curve is the real part of the transform. The r-space vertical scales in each case are the same, and the tic at the center of the vertical axis is the zero point. The transform range is a square window from 3.8 to 12.2 $Å^{-1}$, Gaussian broadened by 0.5 Å. The Cu-Ba spectrum is for four Ba neighbors at 2.61 Å, as for CuI, so that amplitude and phase differences observed in the figure are due only to the difference in backscatter.

the difference in spacing was, of course, taken into account. It is seen in Fig. 2 that, despite the small change in $Z(\Delta Z=3)$, there is a significant phase difference between Cu-I and Cu-Ba. Such a large difference obviously must be accounted for in order to get meaningful results in fits to the data.

A similar procedure was used for Cu-Y ($Z=39$) for which CuBr ($Z=35$) was used. As a check, Zr ($Z=40$) metal data were also used to generate the amplitude and phase for Cu-Y. Both the central atom and backscattering atom had to be corrected using the calculations, from $Z=40$ to $Z=29$ for the central atom and $Z=40$ to 39 for the backscattering atom. No significant spherical-wave correction had to be made for the difference in distance, however, since Zr metal has 12 Zr neighbors at 3.2 Å, the same as the Cu-Y distance. The two starting points, CuBr and Zr metal, resulted in Cu-Y standards that agreed very well with one another, indicating that the procedure has validity.

These standards were used in a multi-Gaussian fit to the second-neighbor region of the Y-Ba-Cu-O samples, starting with the structural parameters from diffraction. Various fits were performed as discussed above for the first-neighbor environment. Constraints and limits were placed on the parameters to reduce the number of variables and to avoid unphysical results. Good fits were obtained. These second-neighbor fit results were then combined with the first-neighbor oxygen fit results to yield starting values for a composite first-plus-second-neighbor fit. This included all the neighbors out to 4 Å. This fit was performed to insure that interference between the first- and second-neighbor regions was not a significant factor. Such was the case since the two procedures gave almost the same structural parameters with good fits to the data. The structural results are discussed in detail below in Sec. IV.

III. NEAR-EDGE RESULTS

The absorption edges for three standards and two Y-Ba-Cu-O samples, low O and high O, are shown in Fig. 3. The standards are Cu_2O, CuO, and $KNa_4[Cu(HIO_6)_2]\cdot 12H_2O$ whose formal oxidation states are Cu I, Cu II, and Cu III, respectively. We had previously[21] used $KCuO_2$ as a Cu III reference compound, but it is hydroscopic and is converted to Cu II on exposure to moisture. This is not the case for the Cu III compound used here. The two Y-Ba-Cu-O samples, low O, $y=6.15$, and high O, $y=6.98$, have mean Cu valences of 1.77 and 2.32, respectively. Since Y-Ba-Cu-O contains two inequivalent Cu atoms, one can expect to have different electronic configurations for the two sites.[29] The different detailed near-edge structures have been discussed extensively,[17–30,36] so we restrict ourselves here to a few comments.

The edge is shifted to higher energies, as expected, when the formal valence is increased for the 1+, 2+, and 3+Cu standards. The pronounced peak at $(E-E_0)=0$ eV in Cu_2O is characteristic of linear, twofold coordinated O-Cu-O configurations. It corresponds to an electric dipole transition from the $1s$ state to empty $4p_{xy}$ states, where the z direction is along the Cu–O bond.

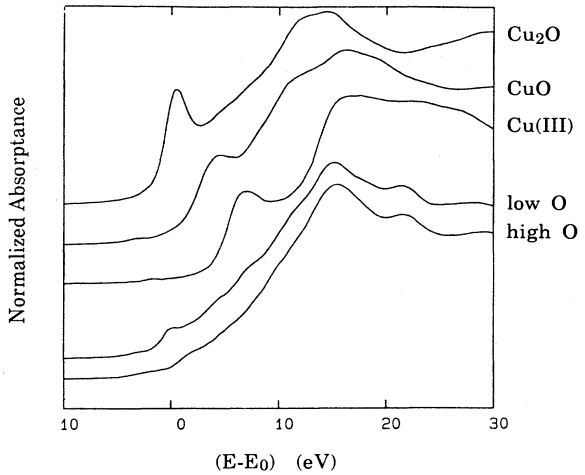

FIG. 3. The Cu near-edge spectra of (from top to bottom) Cu_2O, CuO, a Cu III compound, $KNa_4[Cu(HIO_6)_2]\cdot 12H_2O$ and low-O ($y=6.15$) and high-O ($y=6.98$) Y-Ba-Cu-O. The energy scale is referenced to $E_0=8980$ eV. The vertical scale for each curve is normalized for the same height of the large peak between 10 and 20 eV. The vertical position for each curve is offset and is approximately zero at the intercept of the vertical axis at $(E-E_0)=-10$ eV since the background has been subtracted.

The absorption edge of the superconductors is very broad, covering the entire energy range defined by the I, II, and III formal valence compounds, with the main rise occurring near the II region. The valence in the high O compound $y\approx 7$ consists of a combination of Cu II and Cu III. The Cu II has an electronic configuration of $3d^9$, but the Cu III is not $3d^8$ since this configuration lies below the O p states. Rather the Cu III electronic configuration in both the formally trivalent compounds and in Y-Ba-Cu-O is $3d^9\underline{L}$, where $\underline{L}$ is a hole in the O p band.[25,27,36]

For the oxygen-depleted superconductor, the lower part of the absorption edge is shifted towards lower energy and a pronounced structure occurs at the energy of the Cu_2O ligand peak.[24,27,28,36] This agrees with the result that O is lost from the linear Cu-O chains, leaving O-Cu-O structures. We have also observed this increase in the size of this Cu I peak in fully oxygenated Y-Ba-Cu-O that was heated to 600 °C in a helium atmosphere during the x-ray absorption measurements.[28,33] These results support the conclusion that, as $y=7$ goes to $y=6$, the O is removed from the chains and the Cu(1) becomes monovalent as in Cu_2O with a linear O-Cu-O structural configuration and a $3d^{10}$ electronic configuration.

IV. XAFS RESULTS AND DISCUSSION

A thorough analysis was made of the XAFS data on the Cu edge in each sample. The data were reduced and analyzed as discussed above in Sec. II C. The Fourier transform of the Cu K edge XAFS $k\chi(k)$ to real space is shown in Fig. 4 for $y=6.98$ and 6.15, both at 5 K. The vertical bars on the r axis indicate the position and relative ampli-

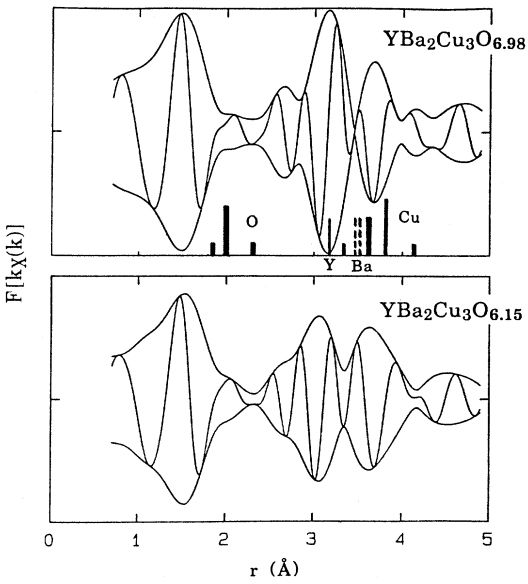

FIG. 4. The Fourier transform of the Cu K-edge XAFS, $k\chi(k)$, to real space for Y-Ba-Cu-O with $y=6.98$ and 6.15, both at 5 K. The transform range is a square window from 3.8 to 12.2 $Å^{-1}$, Gaussian broadened by 0.5 $Å^{-1}$. The envelope curve is the magnitude of the complex transform {plotted as $+|F[k\chi(k)]|$ and $-|F[k\chi(k)]|$} and the oscillatory curve is the real part of the transform. The vertical scales in each case are the same, and the tic at the center of the vertical axis is the zero point. The vertical bars along the r axis indicate the location and relative number of neighbors from the diffraction results (Table I), with the wide bars being O, the medium width, Cu; narrow bars, Y; and dashed, Ba. There is a shift of the XAFS peaks from these positions due to the phase shifts. On this scale, the corresponding bars for the low-O sample would look the same except for the main Cu-O peak at 1.94 Å which would be reduced in height by 20%.

tude of each of the neighbors to the Cu according to the diffraction results, Table I. There is a shift of the XAFS peaks to lower r due to the phase shifts; however, there is a rough correspondence between the two sets of peaks if allowance is made for interference in the XAFS case.

We should mention that the two orthorhombic samples, $y=6.87$ and $y=6.98$, yielded essentially identical spectra over the entire temperature range. This indicates that the local environment is not substantially altered by a small difference in O content. As a result, we will refer to both the $y=6.98$ and $y=6.87$ samples as high-O material. On the other hand, there are significant differences in the spectra for $y=6.98$ and 6.15, as seen in Fig. 4. These difference are evident for both the first-neighbor and second-neighbor regions, which we now discuss.

A. Oxygen first neighbors to Cu and Y

In the region of the first-neighbor oxygen peaks, the low-O sample has fewer O neighbors. Detailed three-Gaussian fits of the Cu-O nearest-neighbor peaks were carried out using a Cu_2O structural standard as discussed above. The number of O neighbors to Cu and their distances, as determined by the XAFS fits, are shown in Table II. The fits were made using a fixed ratio of the number of neighbors for the three first-neighbor peaks according to diffraction results, i.e., 1:5:1 for $y=7$ and 1:4:1 for $y=6$. As seen in Table II, the Cu-O distances are in good agreement with diffraction results. There is only a small discrepancy of a few percent for the long Cu(2)-O(4) bond in both the oxygen-rich and oxygen-deficient Y-Ba-Cu-O and for the short Cu(1)-O(4) bond in the low-O sample. The total weighted number of oxygen neighbors is also in good agreement with diffraction. The XAFS number of neighbors are too large by about 8%. This, however, is well within the uncertainty of the XAFS fits.

The changes in the near-neighbor environment on going from $y=6.98$ to 6.15 are readily apparent. The Cu(2)-O(4) bond length lengthens due to the removal of the O(1) atoms. Since the O(1) atoms contribute to the peak at 1.94 Å, the weighted average number of neighbors in this peak is reduced in the $y=6.15$ sample. The small shortening of the Cu(1)-O(4) bond, however, is not evident in these XAFS fit results.

In addition to the Cu near-neighbor environment, the Y-O environment was examined. The Y K-edge data were analyzed using a Y_2O_3 structural standard, as discussed in Ref. 21. The Y-O coordination number of 8 ± 1 and the average Y-O distance of 2.39 ± 0.01 Å were obtained for all three samples, independent of oxygen content. These results agree with the diffraction numbers. The determination of eight nearest-O neighbors, rather than twelve, with no evidence for another nearby Y-O distance, indicates that no O resides in the Y plane. Also the similarity in the Y-O results for the low-O and high-O samples indicates that the O that is removed on going from $y=7$ to $y=6$ is not the O neighboring the Y atoms, i.e., not the O(2) and O(3). These conclusions again are in agreement with diffraction data and also with our previous results[21] on samples with $y\approx6.85$.

B. Metal and oxygen second neighbors to Cu

As seen in Fig. 4, there are dramatic differences in the spectra between $y=6.15$ and $y=6.98$ for the second-neighbor region, even though the major structural change on going from $y=7$ to $y=6$ is the removal of a first neighbor to a Cu, namely, the O(1) atoms in the chains. With the removal of the O(1) atoms, the a and b axes become equivalent, and the orthorhombic structure becomes tetragonal. As seen in Tables I and II, this change in symmetry does not alter the number of Cu-metal second-neighbor pairs nor does it substantially change their separations since the difference between the a and b lattice constants of the orthorhombic phase is only 0.06 Å. Nonetheless, the second-neighbor peaks in the XAFS spectrum do change substantially. This spectral change is due to a modification of the interference between the various Cu-metal peaks due primarily to a broadening and a movement of the Ba atoms, as discussed below.

A multipeak fit to this second neighbor region was performed. Six Gaussian peaks with variable positions,

TABLE II. Comparison of the diffraction and XAFS results for the room-temperature near-neighbor distances and number of neighbors around the Cu(1) and Cu(2) atoms in orthorhombic $YBa_2Cu_3O_7$ and tetragonal $YBa_2Cu_3O_6$ within a radius of 4 Å. For tetragonal $YBa_2Cu_3O_6$, O(1) of the orthorhombic structure is missing and O(2) and O(3) are equivalent. The notation is from Jorgensen *et al.* (Ref. 10), the structure for $y=7$ from Beno *et al.* (Ref. 3), and the structure for $y=6$ from Torardi *et al.* (Ref. 9). The number of neighbors is the weighted average for the two Cu sites.

	High O ($y=7$)				Low O ($y=6$)			
	Diffraction		XAFS		Diffraction		XAFS	
Cu-X pair	Number of neighbors	r (Å)	Number of neighbors	r (Å)	Number of neighbors	r (Å)	Number of neighbors	r (Å)
Cu(1)-O(4)	0.67	1.85	0.72	1.84	0.67	1.79	0.72	1.83
Cu(1)-O(1) Cu(2)-O(2) Cu(2)-O(3)	3.33	1.94	3.60	1.95	2.67	1.94	2.87	1.95
Cu(2)-O(4)	0.67	2.30	0.72	2.34	0.67	2.46	0.72	2.42
Cu(2)-O(2) Cu(2)-O(3)	2.67	3.66	2.92	3.64	2.67	3.62	2.87	3.66
Cu(2)-Y	2.67	3.20	2.40	3.19	2.67	3.18	2.30	3.16
Cu(2)-Ba	2.67	3.38	2.22	3.37	2.67	3.35	1.90	3.32
Cu(1)-Ba	2.67	3.47	2.22	3.48	2.67	3.57	1.90	3.59
Cu(2)-Cu(2)	0.67	3.37	0.65	3.35	0.67	3.29	0.80	3.35
Cu(2)-Cu(2) Cu(2)-Cu(2) Cu(1)-Cu(1) Cu(1)-Cu(1)	4	3.85	(3.8)	(3.95)	4	3.85	(3.5)	(3.98)

widths and amplitudes were used. The six peaks used the starting amplitudes and positions of Table I: one Cu-O, one CuY, two Cu-Ba, and two Cu-Cu peaks. The amplitudes of the Cu-Ba peaks were allowed to vary but were kept equal to one another. Unlike Ref. 32, we find that combining the two Cu-Ba distances into a single average distance deteriorates the quality of the fit and alters the resulting structural parameters. This is particularly true for the low-O material for which the two Cu-Ba distances differ by 0.2 Å, twice that of the high-O material. An approximation was made for the long Cu-Cu peaks between 3.82 and 3.88 Å: they were treated as a single peak as indicated in Table I. This approximation would be an excellent one if it were not for multiple scattering corrections for one of the pairs and not for the other three pairs.[37] The Cu(1)-Cu(1) pairs along the a axes have no intervening O atoms and so are not effected by multiple scattering. The two planar Cu pairs, Cu(2)-Cu(2) along the a and b axes, are not much affected by multiple scattering due to the puckering of the Cu(2)-O-Cu(2) bonds to an angle of about 170°. The O atoms are enough out of the straight-line path that forward scattering through the O atoms is small. This is not the case for the Cu(1)-Cu(1) pair along the chains, along the b axis. Forward scattering through the intervening O(1) atoms will greatly enhance this peak beyond its one-in-four contribution. Also the phase will be shifted. To account for these effects, we approximated these pairs as a single peak but allowed for a phase shift by varying the threshold energy E_0 and allowing the position and amplitude to go well beyond the structural values from diffraction. This phenomenological approach accounted for the measured peak with an E_0 shift of the Cu metal standard of about -13 eV, a positional shift of about 0.1 Å larger than the diffraction value and an amplitude close to the known weighted average value of four Cu neighbors.

The resulting parameters for these six peaks were then refined by combining them with the three O peak results for the first neighbor region (results of the previous section) into a nine peak fit over the entire region from 1.1 to 3.9 Å. A comparison of the data and the calculated fit is shown at the top of Fig. 5. This refinement did not substantially alter the results of the two-section fit, indicating that the overlap between the first-neighbor O peaks and the second-neighbor metal peaks is not substantial. The refined weighted average number of neighbors and positions for the nine peaks are given in Table II. It is seen that the bond lengths agree quite well with the diffraction results for both the high-O and low-O samples, except for the Cu-Cu peak near 3.85 Å which is shifted to about 3.95 Å due to the multiple scattering discussed above. The weighted number of neighbors are also in good agreement with the diffraction results except for the Cu-Ba peaks which are about 17% too low for the high-O sample and about 30% too small for the low-O material. This discrepancy may be due to inaccuracies in arriving at a Cu-Ba standard, uncertainties in the mean free paths (we used $\lambda=8$ Å for all the samples), and/or anharmonic effects. Some contribution from the latter is very likely, since, as discussed below in Sec. IV C, the Ba position is soft, and its temperature dependence is stronger than that for the other atoms, particularly in the low-O sample.

It is also instructive to show the nine component peaks that fit the spectra in order to see how the individual con-

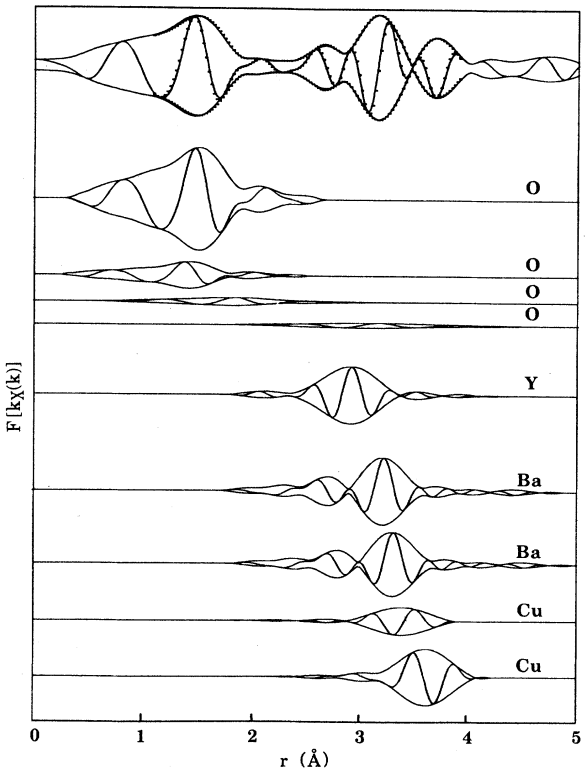

FIG. 5. The Fourier transform of the Cu K-edge XAFS, $k\chi(k)$, for the high-O, $y=6.98$, Y-Ba-Cu-O sample at 5 K. The upper curve is the data (solid curve) and fit (dotted curve). The lower curves are the nine component Cu-X peaks that make up the fit.

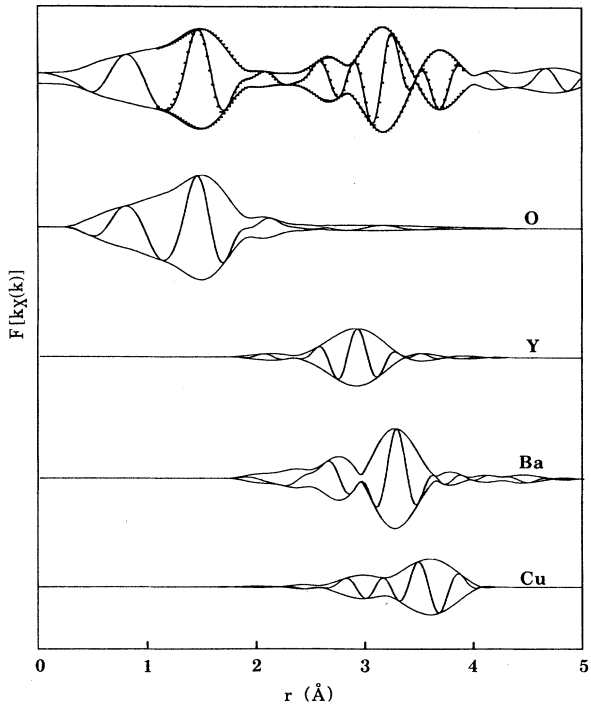

FIG. 6. The Fourier transform of the Cu K-edge XAFS, $k\chi(k)$, for the high-O, $y=6.98$, Y-Ba-Cu-O sample at 5 K. The upper curve is the data (solid curve) and fit (dotted curve). The lower curves are the individual Cu-X contributions due to the neighboring X atoms of the same type that make up the fit.

tributions combine to yield the data and the effects of interference. This is illustrated for the high-O sample, $y=6.98$, at a temperature of 5 K in Fig. 5. It is seen that the O first-neighbor region is dominated by the O(1), O(2), and O(3) neighbors in the a-b plane, all at about 1.94 Å. The short and long Cu-O(4) peaks, the ones due to O atoms along the c axis, make a smaller contribution. In the second-neighbor region, the O makes a negligible contribution compared with the metal atoms. This is also shown in Fig. 6 where the individual contributions due to the neighboring atoms of the same type have been combined. The three peaked second-neighbor feature observed in the data corresponds roughly to the three metal atoms: the Cu-Y, Cu-Ba, and Cu-Cu constituents. These components do, however, strongly overlap and interfere with one another.

The analogous spectra for the low-O material, $y=6.15$, at a temperature of 5 K is presented in Fig. 7. Again, the composite fit accurately accounts for the data in the region from 1.1 to 3.9 Å, as seen in the upper curve. The component peaks are shown below the data. The three-peaked second-neighbor structure for $y=6.98$ (Figs. 5 and 6) becomes two-peaked for $y-6.15$ (Fig. 7) largely due to a reduction in the Cu-Ba peak. This reduction is due to a larger disorder for the two Ba peaks in the low-O material as well as the larger separation of the two component Ba peaks causing more destructive interference. The peak width at 5 K for the low-O material is $\sigma^2\sim 8\times 10^{-3}$ Å^2 compared with $\sigma^2\sim 2\times 10^{-3}$ Å^2 for the high-O material, a substantial difference of $\Delta\sigma^2\approx 6\times 10^{-3}$ Å^2. The absolute value of σ^2 is uncertain due to the lack of a precise determination of the width for the structural standard, modified CuI. However, the difference, $\Delta\sigma^2$, is better determined since the same reference was used in each case. For these low-temperature (5 K) results, some of this difference in width is likely the result of larger static disorder in the low-O material, due possibly to the fact that $y=6.15$ and not 6. The fact that the O content is larger than $y=6$ implies that there are a distribution of local environments giving rise to the large static disorder. This may also be the case for the high O, $y=6.87$ compound, but its disorder is smaller. More importantly, there is a temperature variation in the widths for each compound which is larger for the low-O sample. As a result, this difference in the disorder for the low-O and high-O samples increases to $\Delta\sigma^2\approx 10\times 10^{-3}$ Å^2 at 300 K. In addition to the different Cu-Ba widths and their temperature dependence, there is a similar difference in the splitting of the two Cu-Ba peaks. From Table II, the splitting for low O is larger by $\Delta r\approx 0.16$ Å, compared with the high-O sample. The result of both these effects is a two-peak second-neighbor structure in the data despite the fact that it is composed of several metal-atom neighbors.

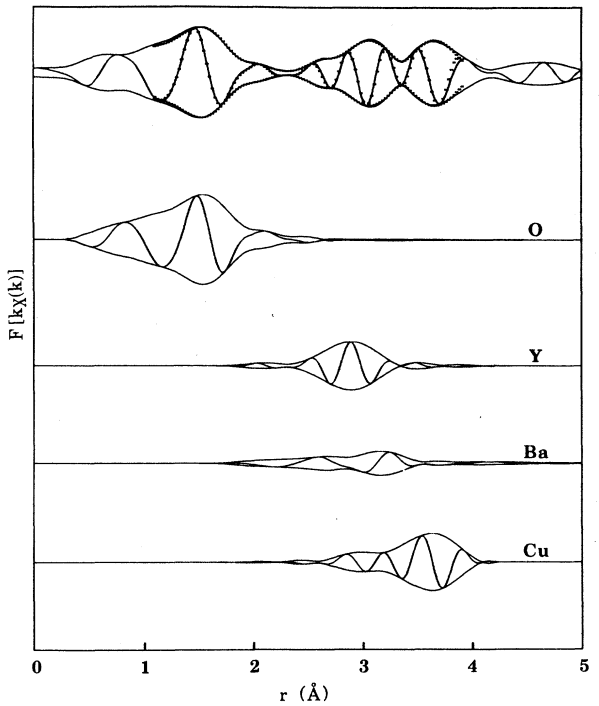

FIG. 7. The Fourier transform of the Cu K-edge XAFS, $k\chi(k)$, for the low-O, $y=6.15$, Y-Ba-Cu-O sample at 5 K. The upper curve is the data (solid curve) and fit (dotted curve). The lower curves are the individual Cu-X contributions due to the neighboring X atoms of the same type that make up the fit. Note the difference in the Ba contributions between this low-O sample and the high-O sample shown in Fig. 6.

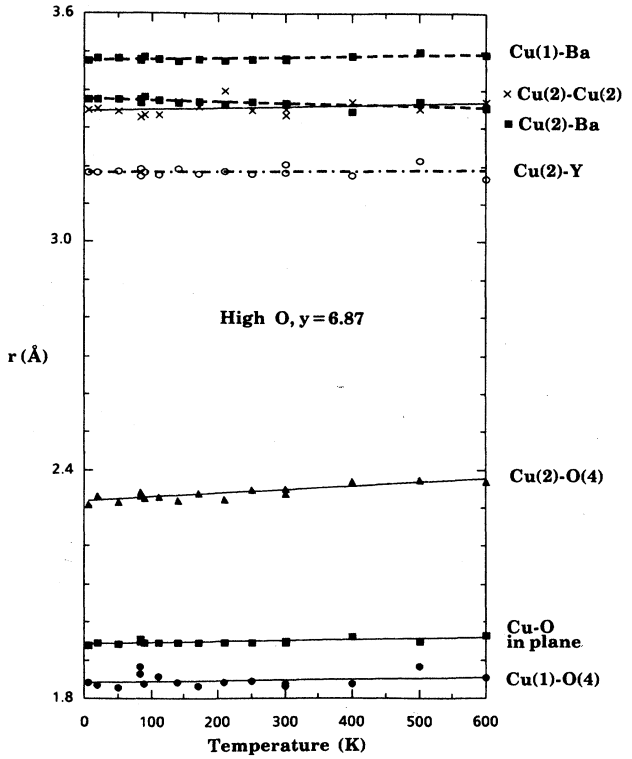

FIG. 8. The temperature dependence of the determined Cu-X near-neighbor distances in high-O Y-Ba-Cu-O for $y=6.87$. Note the temperature variation of the two Cu-Ba distances.

C. Temperature dependence of Cu-X distances

No pronounced shift with temperature was seen in the absorption edge for the Y-Ba-Cu-O samples between 5 and 600 K. Neither was the basic character of the XAFS changed. The changes observed with temperature could all be well accounted for by a smooth change in each of the absorber-to-near-neighbor distances and in the broadening of these distances. Fits, as described above, were performed on all the Cu K-edge data sets for temperatures from 5 to 600 K. The determined Cu-X near-neighbor distances for $y=6.87$ are shown in Fig. 8. Seven of the nine distances of Table II are included in this figure. The long Cu-O distance of about 3.64 Å has a substantial uncertainty due to its large width and smaller contribution (smaller backscattering amplitude) compared with that of the metal atoms. As a result, it is not included. Also excluded is the long Cu-Cu peak near 3.9 Å. It is effected by multiple scattering, as discussed above, and so its near-neighbor spacing is uncertain. This peak, however, had to be included in the fits to the data since it makes a substantial contribution in the fit region for $r<4$ Å, as seen in Fig. 5.

As seen in Fig. 8, the Cu-X distances for $YBa_2Cu_3O_{6.87}$ increase only slightly from 5 to 600 K, except for the shorter of the two Cu-Ba distances. This Cu(2)-Ba spacing decreases with increasing temperature, while the Cu(1)-Ba distance increases. This indicates that, as the temperature increases, the Ba atoms move toward the planes containing the Cu(2) atoms and away from the chains containing the Cu(1) atoms. There is a normal expansion of the lattice, giving rise to the small increases in atomic spacing; but, in addition, there is a distortion of the Ba position within the unit cell as it moves toward the planes. This result is qualitatively consistent with the structural measurements at higher temperature. Comparing the Ba and Cu positions at 300 K (Ref. 3) and at 900 K (Ref. 8), one has that, relative to the Cu(1) position along the c axis at $z=0$, the Ba position moves by $\Delta z=0.005$ while the Cu(2) position moves by a smaller $\Delta z=0.002$. These results indicate that, from 300 to 900 K, the Ba moves away from the Cu(1) and toward the Cu(2), consistent with our results from 5 to 600 K.

Similar features are observed for the Cu-X distances in the low-O ($y=6.15$) sample, as shown in Fig. 9. The actual distances differ somewhat between the high-O and low-O materials, as also indicated in Tables I and II. The temperature variation of the distances is again small except for the Cu-Ba distances. The most striking difference between the low-O and high-O Y-Ba-Cu-O is the overall larger separation between the Cu-Ba peaks and their larger temperature variation for the low-O material. This indicates that the low-O sample has a larger motion of the Ba atoms toward the Cu(2)-O planes with increasing temperature.

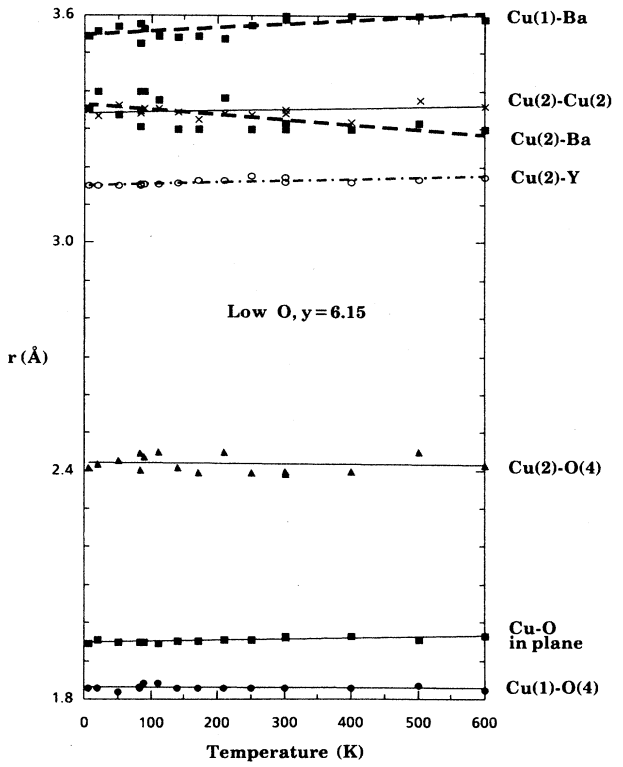

FIG. 9. The temperature dependence of the determined Cu-X near-neighbor distances in low-O Y-Ba-Cu-O for $y=6.15$. Note the stronger temperature variation and larger separation of the two Cu-Ba distances, compared with that for the high-O sample in Fig. 8.

In addition to the large change in Cu-Ba distances with temperature, large increases in the peak widths σ were also observed, as discussed in the previous section. This, coupled with the fact that the determined Ba amplitudes are low (see Table II), implies that anharmonic effects may be significant. Typically, if one fits a symmetric Gaussian peak to a peak that is actually asymmetric due to anharmonicity, one obtains a reduced peak amplitude and a shifted distance.[14,39,43] Anharmonicity could then effect the precise determination of the Ba atomic positions using XAFS. Ba anharmonic motion has been observed in x-ray scattering.[12] There it is pointed out that the Ba atoms lie slightly above the plane of O(4) atoms. The Ba-O distance, which is already short, would be much too short if the Ba atoms were to lie in this plane. This implies that the $-z$ direction is the hard direction for the Ba vibrations, whereas the soft direction is the $+z$ direction, toward the Cu(2)-O planes where the Ba atoms have more room. These facts may account for the observed distortion.

D. Temperature dependence of Cu-O widths

The most substantial changes in the XAFS spectra with temperature could be accounted for by a smooth temperature-dependent broadening of the absorber-to-neighbor distances. This is particularly true for the first-neighbor Cu-O distances which are tightly bound and not much affected by the anharmonicity discussed above for the Ba atoms. A single peak fit was made to the Cu-O peak centered at 1.94 Å. This is the peak that dominates the XAFS first-neighbor spectrum (see Fig. 5) and corresponds to the in-plane Cu-O distances. Although the absolute width squared, σ^2, was not determined, its change with temperature is obtained by comparison of the appropriate peak in the 5-K spectrum to the corresponding peak in the higher-T spectrum. The results for the change in the width squared, $\Delta\sigma^2(T)=\sigma^2(T)-\sigma^2$ (5 K), for the in-plane Cu-O peak for both the low-O and high-O samples are presented in Fig. 10. A smooth variation of $\Delta\sigma^2$ with no dramatic anomalies, such as phonon softening, is observed in this more extensive set of measurements. This is consistent with our earlier results[21] for $y\approx 6.85$ Y-Ba-Cu-O.

From the temperature variation of the observed Debye-Waller-like broadening of the pair distribution functions and the assumption that the individual bonds can be treated as Einstein oscillators, we can estimate[21,41,44] the characteristic vibration frequencies, ω_E, in the crystal using $\sigma^2(T)\approx\hbar/(2\mu\omega_E)\coth(\hbar\omega_E/2k_BT)$, where μ is the reduced mass of the pair of atoms. Fits of these data to the above expression for $\Delta\sigma^2$, with ω_E the only unknown parameter, are shown in Fig. 10. The characteristic Einstein temperatures, $\Theta_E=\hbar\omega_E/k_B$, for the dominant in-plane Cu-O bonds are as follows: $\Theta_E=596\pm 20$ K for the two oxygen-rich samples ($y=6.87$, 6.98) and $\Theta_E=564\pm 20$ K for the oxygen-deficient sample ($y=6.15$). The in-plane Cu-O bonds are 6% softer in the low-O tetragonal Y-Ba-Cu-O than for the fully oxygenated orthorhombic Y-Ba-Cu-O. This small

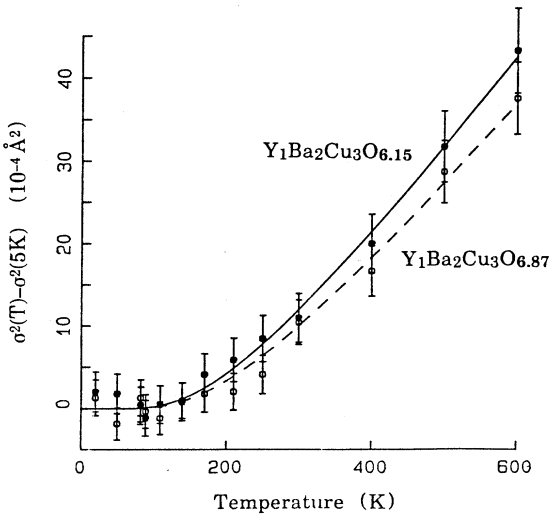

FIG. 10. $\Delta\sigma^2(T)=\sigma^2(T)-\sigma^2$ (5 K) for in-plane Cu-O in Y-Ba-Cu-O with different O content, $y=6.15$ (closed symbols) and $y=6.87$ (open symbols). The solid curves are fits of these data to an Einstein oscillator model, yielding for the characteristic Einstein temperatures $\Theta_E=596\pm 20$ K for the oxygen-rich sample ($y=6.87$) and $\Theta_E=564\pm 20$ K for the oxygen-deficient sample ($y=6.15$).

difference agrees with the expectation that the more disordered oxygen-deficient compound would be somewhat softer for the average Cu-O bond. It is the reverse of the result of Ref. 22. Also for the Cu-Cu pair, we extract a similar difference for the oxygen-rich and oxygen-poor samples.

The data fit an Einstein oscillator model quite well but do show some deviation at low temperatures below $T_c \approx 90$ K (see Fig. 10). The deviations consist of a small increase in $\Delta\sigma^2(T)$ as the temperature is lowered. These differences are at the limits of the error bars, so additional data would be required before any definitive conclusions can be drawn.

V. SUMMARY

We find that, within the experimental error, the XAFS-determined local structure for $YBa_2Cu_3O_y$ agrees well with the long-range order given by diffraction results for both oxygen-rich ($y=6.98$ and 6.87) and oxygen-deficient ($y=6.15$) compounds. The x-ray absorption near-edge structure supports the conclusion that, as $y=7$ goes to $y=6$, the O is removed from the chains and the Cu(1) becomes monovalent as in Cu_2O with a linear O-Cu-O structural configuration and a $3d^{10}$ electronic configuration. For the XAFS analysis, the structural standards determined using spherical-wave corrected experimental data for the Y and Ba neighbors and experimental standards for the O and Cu neighbors provide a good description of the data. These standards work well not only for the first-neighbor O environment but also for the second-neighbor metal-atom environment out to 4 Å. A detailed multipeak analysis reproduced the XAFS spectra well and yielded structural parameters that agree with diffraction.

The temperature dependence of the parameters shows only a smooth variation. No significant anomalies are observed versus temperature. The Cu-X distances have a negligible to a small positive change with temperature, consistent with the lattice expansion. The exception is the Cu-Ba distances which change substantially; the Cu(1)-Ba distance increases and the Cu(2)-Ba distance decreases. This indicates that the Ba moves away from the Cu(1)-O chains and toward the Cu(2)-O planes with increasing temperature and that anharmonicity plays a role. This motion is larger for the oxygen-depleted compound than for the fully oxygenated material. The in-plane Cu-O first-neighbor vibrations exhibit broadening but no significant softening. They agree well with a harmonic, Einstein oscillator model with the characteristic Einstein temperatures $\Theta_E = 596 \pm 20$ K for the oxygen-rich samples ($y=6.98$ and 6.87) and $\Theta_E = 564 \pm 20$ K for the oxygen-deficient sample ($y=6.15$). This indicates that the Cu-O bonds are slightly softer by 6% in the low-O material. Some indication, however, is present for a small increase in $\Delta\sigma^2(T)$ for $T < T_c$, but the signal-to-noise ratio is not adequate to draw any substantial conclusions.

ACKNOWLEDGMENTS

The experiments were performed at Stanford Synchrotron Radiation Laboratory, which is funded by the Department of Energy under Contract No. DE-AC03-82ER-13000, Office of Basic Energy Sciences, Division of Chemical Sciences, and the National Institutes of Health, Biotechnology Resource Program, Division of Research Resources. This research was supported in part by the National Science Foundation Grant No. DMR 85-05549 and the Swedish Natural Science Research Council.

[1]See, for example, *High Temperature Superconductors,* edited by M. B. Brodsky, R. C. Dynes, K. Kitazawa, and H. L. Tuller, Materials Research Symposia Proceedings, Vol. 99 (Materials Research Society, Pittsburgh, 1988); and *Extended Abstracts: High Temperature Superconductors II,* edited by D. W. Capone II, W. H. Butler, B. Batlogg, and C. W. Chu (Materials Research Society, Pittsburgh, 1988), Vol. EA-14.

[2]R. J. Cava, B. Batlogg, R. B. van Dover, D. W. Murphy, S. Sunshine, T. Siegrist, J. P. Remeika, E. A. Reitman, S. Zahurak, and G. P. Espinosa, Phys. Rev. Lett. **58**, 1676 (1987).

[3]M. A. Beno, L. Soderholm, D. W. Capone II, D. G. Hinks, J. D. Jorgensen, J. D. Grace, I. K. Schuller, C. U. Segre, and K. Zhang, Appl. Phys. Lett. **51**, 57 (1987).

[4]T. Siegrist, S. Sunshine, D. W. Murphy, R. J. Cava, and S. M. Zahurak, Phys. Rev. B **35**, 7137 (1987).

[5]R. M. Hazen, L. W. Finger, R. J. Angel, C. T. Prewitt, N. L. Ross, H. K. Mao, C. G. Hadidiacos, P. H. Hor, R. L. Meng, and C. W. Chu, Phys. Rev. B **35**, 7238 (1987).

[6]P. M. Grant, R. B. Beyers, E. M. Engler, G. Lim, S. S. P. Parkin, M. L. Ramirez, V. Y. Lee, A. Nazzal, J. E. Vazquez, and R. J. Savoy, Phys. Rev. B **35**, 7242 (1987).

[7]Y. LePage, W. R. McKinnon, J. M. Tarascon, L. H. Greene, G. W. Hull, and D. M. Huang, Phys. Rev. B **35**, 7245 (1987).

[8]J. D. Jorgensen, M. A. Beno, D. G. Hinks, L. Soderholm, K. J. Volin, R. L. Hitterman, J. D. Grace, I. K. Shuller, C. U. Segre, K. Zhang, and M. S. Kleefisch, Phys. Rev. B **36**, 3608 (1987).

[9]C. C. Torardi, E. M. McCarron, P. E. Bierstedt, A. W. Sleight, and D. E. Cox, Solid State Commun. **64**, 497 (1987).

[10]J. D. Jorgensen, B. W. Veal, W. K. Kwok, G. W. Crabtree, A. Umezawa, L. J. Nowicki, and A. P. Paulikas, Phys. Rev. B **36**, 5731 (1987).

[11]J. S. Swinnea and H. Steinfink, J. Mater. Res. **2**, 424 (1987).

[12]P. Marsh, T. Siegrist, R. M. Fleming, L. F. Schneemeyer, and J. V. Waszczak, Phys. Rev. B **38**, 874 (1988).

[13]P. A. Lee, P. H. Citrin, P. Eisenberger, and B. M. Kincaid, Rev. Mod. Phys. **53**, 769 (1981).

[14]T. M. Hayes and J. B. Boyce, in *Solid State Physics,* edited by H. Ehrenreich, F. Seitz, and D. Turnbull (Academic, New York, 1982), Vol. 37, p. 173.

[15]E. A. Stern and S. M. Heald, in *Handbook on Synchrotron Radiation,* edited by E. E. Koch (North-Holland, New York, 1983), Vol. 1, p. 955.

[16]H. Oyanagi, H. Ihara, T. Matsushita, M. Tokumoto, M. Hirabayashi, N. Terada, K. Senzaki, Y. Kimura, and T. Yao, Jpn.

J. Appl. Phys. **26**, L488 (1987).
[17]J. M. Tranquada, S. M. Heald, A. R. Moodenbaugh, and M. Suenaga, Phys. Rev. B **35**, 7187 (1987); J. M. Tranquada, S. M. Heald, and A. R. Moodenbaugh, *ibid.* **36**, 5263 (1987).
[18]E. E. Alp, G. K. Shenoy, D. G. Hinks, D. W. Capone II, L. Soderholm, H. B. Schuttler, J. Guo, D. E. Ellis, P. A. Montano, and M. Ramanathan, Phys. Rev. B **35**, 7199 (1987).
[19]J. B. Boyce, F. Bridges, T. Claeson, T. H. Geballe, C. W. Chu, and J. M. Tarascon, Phys. Rev. B **35**, 7203 (1987).
[20]H. Oyanagi, H. Ihara, T. Matsushita, M. Tokumoto, M. Hirabayashi, N. Terada, K. Senzaki, Y. Kimura, and T. Yao, Jpn. J. Appl. Phys. **26**, L638 (1987).
[21]J. B. Boyce, F. Bridges, T. Claeson, R. S. Howland, and T. H. Geballe, Phys. Rev. B **36**, 5251 (1987).
[22]H. Oyanagi, H. Ihara, T. Matsubara, T. Matsushita, M. Hirabayashi, M. Tokumoto, K. Murata, N. Terada, K. Senzaki, T. Yao, H. Iwasaki, and Y. Kimura, Jpn. J. Appl. Phys. **26**, L1233 (1987).
[23]G. M. Antonini, C. Calandra, F. Corni, F. C. Matacotta, and M. Sacchi, Europhys. Lett. **4**, 851 (1987).
[24]H. Oyanagi, H. Ihara, T. Matsubara, M. Tokumoto, T. Matsushita, M. Hirabayashi, K. Murata, N. Terada, T. Yao, H. Iwasaki, and Y. Kimura, Jpn. J. Appl. Phys. **26**, L1561 (1987).
[25]A. Bianconi, A. Congiu Castellano, M. De Santis, C. Politis, A. Marcelli, S. Mobilo, and A. Savoia, Z. Phys. B **67**, 307 (1987).
[26]E. D. Crozier, N. Alberding, K. R. Bauchspiess, A. J. Seary, and S. Gygax, Phys. Rev. B **36**, 8288 (1987).
[27]F. Baudelet, G. Collin, E. Dartyge, A. Fontaine, J. P. Kappler, G. Krill, J. P. Itie, J. Jegoudez, M. Maurer, Ph. Monod, A. Revcolevschi, H. Tolentino, G. Tourillon, and M. Verdaguer, Z. Phys. B **69**, 141 (1987).
[28]J. B. Boyce, F. Bridges, T. Claeson, and T. H. Geballe, Phys. Scr. **37**, 912 (1988).
[29]S. M. Heald, J. M. Tranquada, A. R. Moodenbaugh, and Y. Xu, in *High Temperature Superconductors,* edited by M. B. Brodsky, R. C. Dynes, K. Kitazawa, and H. L. Tuller, Materials Research Symposia Proceedings, Vol. 99 (Materials Research Society, Pittsburgh, 1988), p. 757.
[30]F. W. Lytle, R. B. Greegor, and A. J. Parson, Phys. Rev. B **37**, 1550 (1988).
[31]K. Zhang, G. B. Bunker, G. Zhang, Z. X. Zhao, L. Q. Chen, and Y. Z. Huang, Phys. Rev. B **37**, 3375 (1988).
[32]S. J. Gurman, G. Diakun, B. Dobson, S. Abell, G. N. Greaves, and R. Jordan, J. Phys. C **21**, L475 (1988).
[33]J. B. Boyce, F. Bridges, T. Claeson, R. S. Howland, and T. H. Geballe, in Ref. 29, p. 943.
[34]C. Y. Yang, S. M. Heald, J. M. Tranquada, A. R. Moodenbaugh, and Y. Xu, Phys. Rev. B **38**, 6568 (1988).
[35]J. B. Boyce, F. Bridges, T. Claeson, R. S. Howland, T. H. Geballe, and M. Nygren, in *Extended Abstracts: High Temperature Superconductors II,* edited by D. W. Capone II, W. H. Butler, B. Batlogg, and C. W. Chu (Materials Research Society, Pittsburgh, 1988), Vol. EA-14, p. 221.
[36]A. Fontaine, A. Bianconi, A. M. Flank, E. Dartyge, G. Krill, P. Lagarde, M. Maurer, H. Tolentino, and G. Tourillon (unpublished).
[37]E. D. Crozier, N. Alberding, K. R. Bauchspiess, A. J. Seary, S. Gygax, R. Ingalls, and B. Hauser (unpublished).
[38]F. Bridges, Nucl. Instrum. Methods Phys. Res. Sect. A **257**, 447 (1987).
[39]J. B. Boyce, T. M. Hayes, and J. C. Mikkelsen, Jr., Phys. Rev. B **23**, 2876 (1981).
[40]J. B. Boyce, J. C. Mikkelsen, Jr., F. Bridges, and T. Egami, Phys. Rev. B **33**, 7314 (1986).
[41]J. B. Boyce, F. Bridges, T. Claeson, T. H. Geballe, G. W. Hull, N. Kitamura, and F. Weiss, Phys. Rev. B **37**, 54 (1988).
[42]A. G. McKale, B. W. Veal, A. P. Paulikas, S.-K. Chan, and G. S. Knapp, J. Am. Chem. Soc. **110**, 3763 (1988).
[43]P. Eisenberger and G. S. Brown, Solid State Commun. **29**, 481 (1979).
[44]E. Sevillano, H. Meuth, and J. J. Rehr, Phys. Rev. B **20**, 4908 (1979).